# Temperature effects of bifacial modules

## Hotter or cooler?

Lamers, M.W.P.E.; Özkalay, E.; Gali, R. S.R.; Janssen, G. J.M.; Weeber, A. W.; Romijn, I. G.; Van Aken, B. B.

**Important note**
To cite this publication, please use the final published version (if applicable).
Please check the document version above.
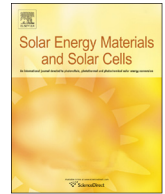
# Temperature effects of bifacial modules: Hotter or cooler?

M.W.P.E. Lamers[a], E. Özkalay[a], R.S.R. Gali[a], G.J.M. Janssen[a], A.W. Weeber[a,b], I.G. Romijn[a], B.B. Van Aken[a,*]

[a] *ECN part of TNO – Solar Energy, Westerduinweg 3, 1755 LE Petten, The Netherlands*
[b] *Delft University of Technology, PVMD Group, Mekelweg 4, 2628 CD Delft, The Netherlands*

## ARTICLE INFO

## ABSTRACT

In this paper we show the results from indoor and outdoor measurements on solar cells and modules, manufactured with different bifacial and monofacial cell architectures and encapsulated in different configurations. Reflection/transmission, IV and IQE spectra of single-cell laminates were measured and used to determine the energy spectra for all heat loss and absorption processes, including thermalisation, recombination, entropy generation, parasitic absorption and electrical power generation. From these spectra, the effective heat input was calculated for front, rear and combined irradiance. The power output, bifacial gain and module operating temperature were monitored of single-cell laminates exposed to indoor irradiance as well as of full-size modules installed on our rooftop.

We have found that the effective heat input for bifacial glass-glass modules is increasingly larger with increasing rear irradiance compared to monofacial modules. Measured temperatures of rooftop-installed modules strongly indicate that the effective heat transfer coefficient of glass-glass modules is higher than that of white back sheet modules. The observed combined effect of heat input and heat transfer is that only at rear irradiance fractions beyond 15% the additional heat input can cause the bifacial modules to be hotter than their monofacial counterpart, but the energy yield is still much higher due to the large bifacial gain. In the case of moderate albedo, the bifacial energy gain is not accompanied by a higher temperature of the bifacial module compared to the monofacial module.

## 1. Introduction

Bifacial cells and modules collect light falling on the front-side of the panels, but also collect light falling on the rear. This will increase the total irradiance absorbed by the panel, and the current generated by the panels increases accordingly. One of the remaining research questions is whether bifacial solar panels operate at higher or at lower temperatures than monofacial panels. One side of the argument is that the extra light absorption increases the module temperature, which will negatively affect the total power output of the panels and reduce the effective bifacial yield gain. On the other hand, as the infrared (IR) light transmission through the panels is also higher [1], it can be argued that the panels will be cooler. Also, Hezel showed that in a bifacial PV panel with about one cell's width spacing between the bifacial solar cells, the temperature is lower compared to densely packed monofacial module [2]. Excess heat has a negative effect on the power output of photovoltaic (PV) modules, as the $V_{oc}$ decreases with increasing solar cell temperature [3,4]. Optoelectric properties of the cell and the module materials are critical parameters for the module temperature under operating conditions. The heat balance in a PV module is affected by three main factors: i) irradiance that is absorbed, transmitted or reflected; ii) conversion losses either by thermalisation, entropy generation, recombination or parasitic absorbance [5,6] and iii) heat losses by radiation and convection. The irradiance that enters the cell is absorbed or transmitted through the cell. The light that is transmitted through a cell, mostly (near-)IR light, is either transmitted out of the module, absorbed by the module materials or reflected back to the cell. Module materials are, for example, polymer back sheet or rear glass panel. The irradiance absorbed by the cell will be partly used to produce electricity but will also produce heat due to the conversion losses, described above.

In this work we will show the contribution of these thermal processes to the heat balance and the actual (working) temperature of the module. First, we analyse the spectral dependence of the optical and electrical behaviour of different solar cell architectures and single-cell laminates in laboratory. Then, the effective heat input is determined. The heat transfer coefficient is determined for monofacial and bifacial modules under controlled indoor conditions. Also, the effect of

---

additional rear illumination on the overall heat balance of the different single-cell laminates is presented. Subsequently, we analyse outdoor data of the single-cell laminates and confirm the results by a comparison with commercial modules on a flat rooftop.
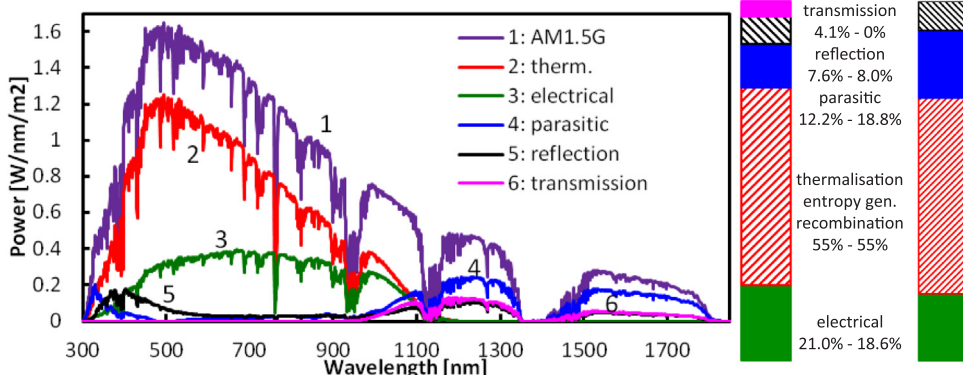
## 2. Experimental section

Monofacial white back sheet and bifacial glass-glass single-cell laminates were manufactured; both types of modules were made with monofacial Al-BSF and with bifacial n-PERT solar cells. The Al-BSF solar cell is the conventional solar cell made on 243 cm$^2$ p-type silicon wafer. The n-type doped emitter layer is produced by diffusion of phosphorus using a tube furnace. The highly doped BSF layer is formed by alloying with an Al layer applied by screen-printing. A SiN$_x$ layer is used for passivation and anti-reflective purposes on the front side of the solar cell. H-pattern metallisation on the front and three busbars on the rear are printed and fired to allow contacting and interconnection.

n-PERT solar cells (Czochralski-silicon, M0 wafers, 239 cm$^2$) are manufactured with standard processes on industrial tools as reported before [7,8]. Random pyramid texture is obtained with alkaline wafer etching. The diffused emitter and BSF are processed using industrial tube furnaces by Tempress [9]. The emitter is made using BBr$_3$ as precursor, the BSF is made using POCl$_3$ as precursor. The additional lateral conductivity in the phosphorus doped BSF contributes to a good FF despite the open rear side metallisation and increases the tolerance to high substrate resistivities. SiN$_x$ layers for passivation and AR-coating purposes are deposited on the front and on the rear side. Screen or stencil printing can be used to apply the front and rear side metallisation grids. Both metallisation grids are fired in a single step in an IR-heated belt furnace.

Single-cell laminates were made by soldering tabs to the busbars of the solar cells. The cross-connected tabs on either side of the solar cell were contacted with two additional tabs to allow four-point measurements. Solar glass was used as front panel. Rear panel was either white back sheet or the same type of glass as on the front side. Fast-cure EVA was used as encapsulant.

Current-voltage (I-V) measurements have been conducted with a Class AAA solar simulator (Wacom) on a non-conductive, low reflective (anodised) chuck according to the IEC standard [10] under standard test conditions: 1000 W/m$^2$ with AM1.5 G spectrum, 25 °C. I-V measurements of the solar modules are measured by a category "class A" flash tester PASAN IIIb sun simulator, in accordance with IEC 60904-9.

Reflection and transmission of the cells, single-cell laminates and module materials are measured using the integrating sphere Labsphere RTC 060 SF. The wavelength range is 330–1750 nm. The reflection and transmission spectra are obtained by convolution of the relative reflection and transmission measurement with the reference AM1.5G spectrum. The absorption spectrum is calculated from the difference between the AM1.5G spectrum and the reflection and transmission spectra.

Spectral response is measured using a xenon lamp in combination with a filter wheel to excite the samples. Bias light is added to put the samples under testing in operational conditions. The filter wheel contains 32 optical band pass filters which have different wavelengths from 330 nm to 1200 nm.

The energy spectrum of the sum of the electrical power and the thermalisation, recombination, resistive and entropy generation losses is given by the convolution of the absorption spectrum with the IQE curve and the solar spectrum. The electrical power spectrum is this spectrum multiplied with the ratio $E_{g,mpp}$ / $E(\lambda)$, where $E_{g,mpp}$ is the energy corresponding to the maximum power point voltage and $E(\lambda)$ the energy of a photon with wavelength $\lambda$; the thermalisation spectrum with the ratio $(E(\lambda)-E_g)$ / $E(\lambda)$, with $E_g$ the band gap energy of Si and the remaining loss spectrum with the ratio $(E_g-E_{g,mpp})$ / $E(\lambda)$. Finally, the parasitic heating is given by the absorption spectrum minus the power and loss spectra.

The outdoor measurement set-up consists of a south-facing tilted rack, that is open to the rear side. $V_{oc}$, $I_{sc}$ and temperature of single-cell laminates were measured every 10 min in quick succession. To ensure the conditions are (nearly) identical for each measurement sequence, the in-plane irradiance was measured a few times before, in-between and after these single-cell measurements. In case the irradiance measurements within a sequence deviates too much, that data sequence was rejected. In-between the measurement sequences, all single-cell laminates were put under a passive load to mimic maximum power point conditions.

Also, the rooftop system on ECN.TNO's building was used to study the performance and actual temperature of commercial 60-cell modules. These measurements were also done in 10-min intervals, but all data and I-V curves were recorded simultaneously in 1 s. Details of that system have been reported before [11].

## 3. Results and discussion

### 3.1. Indoor characterisation to determine the heat input for solar cells

Two different cell architectures, including monofacial p-type Al-BSF and bifacial n-type PERT solar cells [12,13] were analysed using I-V, reflection, transmission and spectral response data. From these data, the spectral response of each cell over the AM1.5G spectrum is divided in generation of electric power, thermalisation, recombination and entropy generation losses, parasitic absorption and optical losses. Parasitic absorption includes free carrier absorption [5] and absorption by metal and module materials.

As example, the spectral analysis for an n-PERT solar cell is shown in Fig. 1. The thermalisation losses decrease steadily with increasing wavelength as the corresponding photon energy decreases towards the band gap energy of Si, i.e. 1.1 eV corresponding to 1100 nm. Consequently, at wavelengths above 1050 nm, near and above the bandgap, parasitic absorption becomes the dominant effect.



**Fig. 1.** Spectral distribution of electrical output and various loss mechanisms of an n-PERT solar cell; numbers in legend are used to distinguish the spectra. "therm." Stands for the thermalisation, recombination and entropy generation losses. The bars on the right-hand show the relative parts of the total energy for an n-PERT and an Al-BSF solar cell; same colours are used in both graphs. (For interpretation of the references to color in this figure legend, the reader is referred to the web version of this article.).
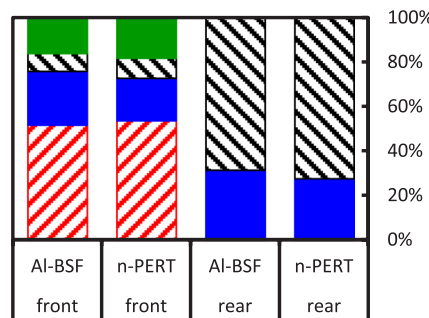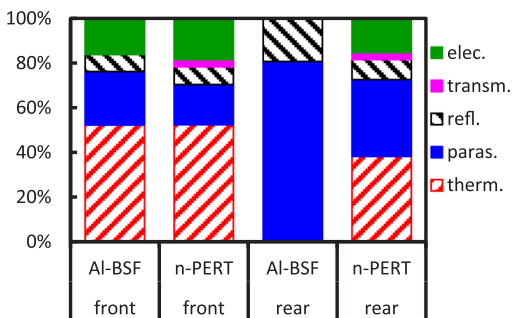
**Fig. 2.** Distribution of incident energy over five possible processes: (top to bottom) electrical energy, transmission, reflection, parasitic heating and "therm." which are the conversion losses, consisting of thermalisation, entropy generation and recombination. The distributions are given for white back sheet (left) and glass-glass modules (right) with the cell type and irradiated side as indicated under the bars. The effective heat input is the total of the "paras." and "therm." contributions.

### 3.2. Indoor characterisation to determine heat input for single-cell laminates

The analysis on I-V, reflection, transmission and spectral response data were again performed after encapsulation. Fig. 2 (left) shows the distribution over the categories for front and rear irradiance of glass-glass (g-g) laminates for Al-BSF and n-PERT cells. Striking is the large parasitic heating for the Al-BSF [6] and for the rear side of the bifacial solar cells, due to absorption in layers on the rear. The effective heat input is shown for the laminates with g-g or white back sheet, Fig. 2 (right). For 1000 W/m² monofacial irradiance, the effective heat input for laminates with Al-BSF solar cells (red bars) is larger than for laminates with n-PERT solar cells (blue bars). Nevertheless, all laminates show 70–76% of the incident light converted to heat, comparable values were calculated from the cell analysis (not shown).

Fig. 2 shows the distribution of incident energy for single-sided, 1-sun irradiance only. The effective heat input consists of the parasitic heating (blue parts) and the recombination, thermalisation and entropy generation losses (red parts). The effective heat input for both sides of glass-glass modules and the front side of the white back sheet modules is between 700 and 760 W/m². However, this is not the complete story, as for free-standing systems, light falls on both sides of the solar module simultaneously. The same analysis was performed for additional irradiance on the rear side of all laminates with data and parameters corresponding to the rear side characteristics.

Under steady-state conditions, the module temperature is given by

$$T_m = T_{amb} + \frac{\alpha_f G_{front} + \alpha_r G_{rear}}{U}, \tag{1}$$

where the net absorption coefficient $\alpha_f$, $\alpha_r$ is given by $\alpha_i = 1 - R_i - T_i - \eta_i$, with $R_i$, $T_i$ and $\eta_i$ the reflection, transmission and power conversion efficiency of side $i$, and $U$ is the heat transfer coefficient in W/m²/K. The effective heat input $Q_i$, i.e. the sum of the thermal and parasitic parts in Fig. 2, is equivalent to the term $\alpha_i G_i$ in Eq. (1). The bifacial or total effective heat input is then given by

$$Q_{tot} = \alpha_f G_{front} + \alpha_r G_{rear}. \tag{2}$$

In Fig. 3, the bifacial effective heat input was calculated for 1000 W/m² on the front and an additional 100 W/m² (bifacial 10%) or 200 W/m² (20%) on the rear. Note that for the white back sheet modules ≈ 30% of the incident light is absorbed by the back sheet and contributes to the heating of the modules.

Under monofacial irradiance, i.e. 0% rear irradiance, glass-glass single-cell laminates have the same or lower effective heat input compared to laminates with white back sheet. With increasing rear irradiance, the effective heat input increases. The rate of increase is significantly higher for bifacial glass-glass modules than for monofacial white back sheet modules as $Q_{rear}$ is larger. Note that there is a cross-over point for the n-PERT modules. Below 6% additional rear irradiance, $Q_{total}$ is larger for white back sheet modules. Above that point $Q_{total}$ is higher for glass-glass modules. As a result, at 20% rear irradiance additional to the 1000 W/m² front irradiance, the glass-glass module with monofacial solar cells has a 12% higher effective heat input compared to its white back sheet counterpart. Also, the glass-glass
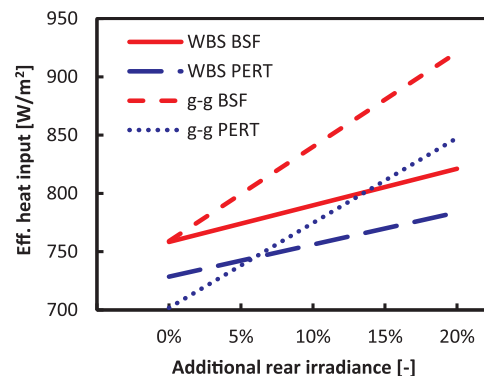


**Fig. 3.** Effective heat input for monofacial and bifacial laminates as a function of additional rear irradiance at constant 1000 W/m² front irradiance. WBS stands for white back sheet, g-g for glass-glass modules.

module with the bifacial n-PERT solar cell, whose heating input at front irradiance only was 4% lower, shows an 8% higher effective heat input under bifacial conditions.

### 3.3. Indoor heating of single-cell laminates to determine heat transfer coefficient

Single-cell laminates with bifacial n-PERT solar cells were exposed to 1000 W/m² irradiance under an EternalSun steady state solar simulator [14]. I-V curves and module temperature were recorded every 10 s. Temperature was determined with PT-100 thermocouple stuck to the rear of the module. Fig. 4 shows the measured module temperature as a function of the heating time for two different module configurations. The data were fitted to an exponential heating equation:

$$T(t) = T_{amb} + a(1 - \exp(-bt)), \tag{3}$$

where $T(t)$ is the time-dependent temperature, $T_{amb}$ is the ambient temperature and $a$ and $b$ are fit parameters. Parameter $a$ describes the



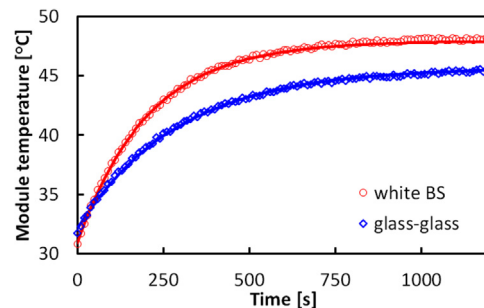**Fig. 4.** Module temperature as a function of the time exposed to 1000 W/m² irradiance for (red) white back sheet and (blue) glass-glass single-cell laminates, both with bifacial solar cells. Solid lines are fitted to the exponential heating equation, see main text. (For interpretation of the references to color in this figure legend, the reader is referred to the web version of this article.).

**Table 1**
Fitted and calculated values for the heating curves of Fig. 4.

| | $T_{ss}$ [°C] | $Q$ [W/m$^2$] | $U$ [W/m$^2$/K] | $t_{1/2}$ [s] | $C_p$ [kJ/m$^2$/K] | $C_p$ from [15] [kJ/m$^2$/K] |
|---|---|---|---|---|---|---|
| white BS | 47.9 | 729 | 29.5 | 140 | 6.5 | 6.6 |
| glass-glass | 45.7 | 702 | 31.3 | 200 | 9.9 | 10.1 |

steady state situation with $a$ equal to the difference between the steady state temperature $T_{ss}$ and ambient temperature. Under constant irradiance and ambient conditions, $a$ is given by $Q / U$ where $Q$ is the heat source term in W/m$^2$. Fit parameter $b$ determines the heating rate and is given by $U / C_p$, where $C_p$ is the heat capacity in J/m$^2$/K.

$T_{ss}$ for the glass-glass module is about 46 °C, compared to 48 °C for the white back sheet module. From the data shown in Fig. 2, the respective heat source values $Q$ are determined, see Table 1. Taking the fitted values for $a$ and calculated values for $Q$, the heat transfer coefficient is calculated. The exponential fit also allows to describe the heating (or cooling) with a half-time $t_{1/2}$ where $t_{1/2}$ is equal to ln(2)/$b$. In Fig. 4 the heating rate for the white back sheet module is clearly faster, and thus the half-time for that module is significantly shorter than for the glass-glass module with $t_{1/2}$ = 140 s and $t_{1/2}$ = 200 s, respectively. Applying the values for $U$ and $b$, the heat capacity $C_p$ is derived. The heat capacity is also calculated, based on the bill of materials and reported values for the specific heat capacity [15], and compared with the experimental values, as can be seen in the last two columns of Table 1. The good agreement between the calculated values and the experimentally derived values for $C_p$. are a validation of the thermal model for the heating curve and its consistency with the determined values for the effective heat input, as shown in Fig. 2.

Although under these indoor conditions the glass-glass laminate showed a 2.2 °C lower heating at 1000 W/m$^2$ irradiance, care should be taken when translating these results to outdoor conditions. Amongst others wind and relative humidity will influence the heat transfer coefficient $U$, whereas the effective heat source term $Q$ will be modified by the total irradiance and the ratio between front and rear irradiance, as is most relevant for outdoor conditions.

### 3.4. Outdoor analysis of single-cell laminates

The laminates are installed on a rooftop rack. For our experiment, the rear irradiance is on average $\approx$ 11% of the front irradiance but varies a lot. $V_{oc}$ and $I_{sc}$ are logged every ten minutes; in-between the modules are put under a load to simulate working conditions. The effective irradiance $G_{eff}$ is deduced from the measured $I_{sc}$ according to $G_{eff} = I_{sc,meas} / I_{sc,STC} \times 1000$ W/m$^2$. The actual solar cell temperature can be calculated from the irradiance and the measured $V_{oc}$ using single diode fit parameters.

Fig. 5 shows the difference between the module temperature and the ambient temperature for different module architectures. The module configurations depicted in the figure are the ones with Al-BSF

and n-PERT solar cells and using, at the rear side, a white back sheet (left) or glass panel (right). For a given module configuration, which means that the heat transfer coefficient $U$ is the same, the modules with bifacial solar cells have lower temperatures than the ones with Al-BSF solar cells. This is in good agreement with the calculated behaviour shown in Fig. 3.

Comparing the two different module configurations, both the heat transfer coefficient $U$ and the effective heat input $Q$ are different. Fig. 5 shows that the module temperature for white back sheet laminates is higher than for g-g laminates. This is unexpected from the effective heat input $Q$ as Fig. 3 shows that $Q$ under bifacial irradiance for g-g laminates is larger than for white back sheet laminates, independent on cell type. However, the steady state module temperature is determined by the ratio $Q/U$, see Eqs. (1) and (2). The heat transfer coefficient $U$ for g-g laminates is also larger than that for white back sheet laminates, see Fig. 4 and Table 1. This indicates that the effective heat transfer of g-g laminates compared to white back sheet laminates is more than large enough to compensate the difference in heat input. This can be partly explained by the radiative losses as the emissivity of glass is 6% higher than for back sheet. Also, the heat transfers through the module materials and from the (rear) panels to air are different.

Finally, note that the difference in module temperature between monofacial Al-BSF and bifacial n-PERT laminates at 1000 W/m$^2$ is 4 °C. Taking the values for Q from Fig. 3 at about 10% rear irradiance, this temperature difference under outdoor conditions can be explained if the $U$ value of the g-g laminate is only 8% higher than the value given in Table 1.

### 3.5. Outdoor analysis of commercial modules

The lower temperature for g-g laminates relative to white back sheet laminates is confirmed by observations on commercial white back sheet and g-g modules with the same cell architecture. The only difference is the absence of a frame for the g-g laminates. Fig. 6 shows the difference in $I_{sc}$, $V_{oc}$ and module temperature for the bifacial modules compared to the monofacial ones. For the bifacial ones, the average $I_{sc}$ increase of 0.2 A at 100 W/m$^2$ corresponds to a bifacial gain of 25% due to rear side light collection. The average $I_{sc}$ increase at 1000 W/m$^2$ of 0.8 A indicates a bifacial gain of 8%. The $V_{oc}$ for bifacial modules at low irradiance is much higher, due to the high rear side contribution and the strong dependence of $V_{oc}$ on irradiance in this regime. At high irradiance the bifacial module has a nearly constant higher voltage.

With increasing front irradiance, the monofacial module temperature increases, more or less, linearly with 3 K per 100 W/m$^2$, consistent with a value of U around 33 W/m$^2$/K. The right-hand side of Fig. 6 shows the difference in module temperature between the bifacial and the monofacial module. Although there is quite some scatter on the data, due to e.g. variation in wind, rear:front irradiance distribution and angle of incidence, there is a clear trend in the data. At low irradiance, which corresponds to 25–35% rear irradiance, the bifacial module is up to 1 K warmer than the monofacial module. This condition
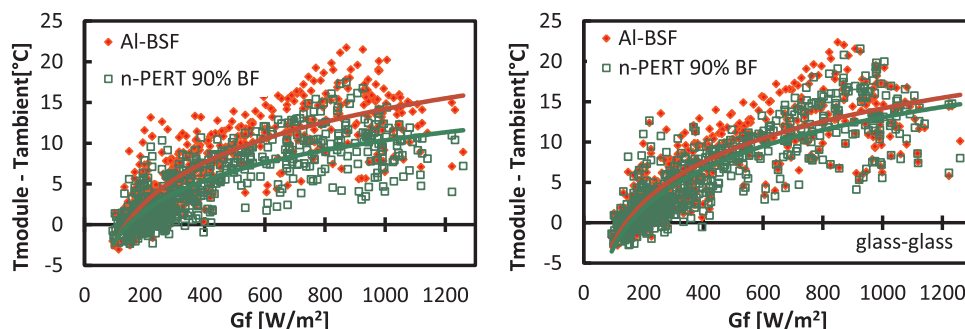


**Fig. 5.** Difference between module temperatures and ambient temperature for Al-BSF and n-PERT cells in white back sheet (left) and g-g (right) laminates.
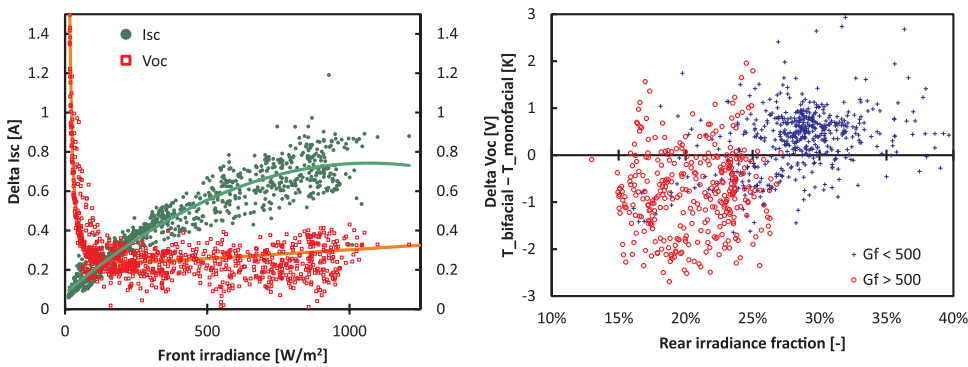
**Fig. 6.** Increase in $I_{sc}$ and $V_{oc}$ for a commercial, bifacial module compared to its monofacial counterpart. The modules are rack mounted, south-facing at 30° tilt with low albedo. Solid lines are guides to the eye. (right) the difference in module temperature as a function of the rear irradiance fraction. Data is divided in low irradiance with Gf below 500 W/m² and high irradiance with Gf larger than 500 W/m².

is mostly associated with a relatively large bifacial power gain. At higher irradiances, when the rear irradiance is less than 25%, most of the data points show that the bifacial module is between 0 and 2.5 K cooler than the monofacial module. These conditions correspond to on average, an 8% bifacial gain in output power.

These results are in fair agreement with the heat input as shown in Fig. 3, blue lines, where the bifacial n-PERT module absorbs more heat above 6% rear irradiance and the monofacial n-PERT module absorbs more heat below 6% rear irradiance. The cross-over point for the module operating temperature is determined both by the heat input and the heat transfer coefficient of the modules. If, as predicted from the data of Fig. 5 on single-cell laminates, the heat transfer coefficient of g-g modules with n-PERT solar cells is larger than of modules with a white back sheet, the cross-over point of the module temperature will be beyond the 6% rear irradiance fraction, in agreement with Fig. 6 (right).

Note, that the cross-over point of hotter or cooler operation of bifacial n-PERT modules compared to monofacial modules depends strongly on which module materials are being considered. For commercial monofacial Al-BSF modules with white back sheet the effective heat input line (solid red line in Fig. 3) crosses the line for the bifacial n-PERT module at about 8% rear irradiance fraction. Thus, it is expected that the monofacial Al-BSF modules with white back sheet will only be cooler than the bifacial al n-PERT modules at a rear irradiance fraction even higher than the 25% observed for the monofacial n-PERT module. This corresponds, typically, to conditions with irradiance significantly below 500 W/m².

If the white, reflecting back sheet of monofacial modules were to be replaced by absorbing black back sheet, e.g. for aesthetic reasons, the increase of heat input of the monofacial module with rear irradiance would be even stronger and the bifacial module would be cooler under most irradiance conditions.

## 4. Conclusions

A full analysis of bifacial and monofacial solar cells and modules is made to determine how the energy of the solar spectrum is distributed. For the n-PERT solar cell two-thirds of the energy is converted to heat via conversion losses (thermalisation, entropy generation and recombination) and parasitic losses (absorption in module materials, metal, free carrier absorption). On module level, 70–76% of the incident light is converted to heat with the highest value for the rear side absorption in the Al-BSF of monofacial solar cells in glass-glass modules. Note that in white back sheet modules, absorption by the opaque back sheet also converts 30% of the incident light to heat. Based on lab measurements, a combination of front and rear irradiance yields a strong increase in the effective heat input for glass-glass modules, irrespective of solar cell architecture. Likewise, for white back sheet modules this increase is much smaller for both monofacial and bifacial solar cells.

Constant front irradiance test in the lab shows that white back sheet

modules do become 2 K warmer than glass-glass modules. This was not only due to the lower heat input but also due to a higher heat transport coefficient U of the g-g modules. Moreover, we found that the half-time towards steady-state temperature is 140 s for the back sheet modules, whereas the half-time for glass-glass modules is 200 s. By combining fitted heat transfer coefficients U with the observed heating curves under constant irradiance and heat input we derive values for the heat capacity of these modules that are in good agreement with values based on the bill of materials and literature values of the individual materials [15], validating the effective heat input and module temperature models.

Outdoor analysis of single-cell laminates and commercial modules yield that despite the higher effective heat input for glass-glass modules under real, bifacial operating conditions, the module temperature is still lower, especially under high irradiance conditions. This can again be ascribed to a higher U value of glass-glass modules. Under low irradiance conditions, when due to high diffuse component in the irradiance the fraction rear irradiance is high and the bifacial power output gain is around 20%, the increase in light absorption increases the bifacial module temperature by up to 1 K. On the other hand, under high irradiance bifacial modules are cooler than monofacial modules despite the higher power output and higher effective heat input.

To conclude, even in cases where high rear irradiance leads to warmer bifacial modules, the gain due to the bifaciality is much higher than losses due to slight heating. Changes in the bill of materials, e.g. thinner glass, thereby increasing the effective heat transfer *U* may further decrease the steady state temperature of the bifacial PV panels relative to monofacial ones, even under high albedo conditions.

## Appendix A. Supporting information

Supplementary data associated with this article can be found in the online version at http://dx.doi.org/10.1016/j.solmat.2018.05.033.

## References

[1] C.Z. Zhou, P.J. Verlinden, R.A. Crane, R.M. Swanson, R.A. Sinton, 21.9% efficient silicon bifacial solar cells, in: Proceedings of Conf. Rec. 26th IEEE Photovoltaic Specialists Conference, IEEE, 1997, pp. 287–290 ⟨http://dx.doi.org/10.1109/PVSC.1997.654085⟩.

[2] R. Hezel, Novel applications of bifacial solar cells, Photovolt. Res. Appl. 11 (2003) 549–556, http://dx.doi.org/10.1002/pip.510.

[3] T. Tiedje, E.D.C.G. Yablonovitch, B.G. Brooks, Limiting efficiency of silicon solar cells, IEEE Trans. Electron Devices 31 (1984) 711–716.

[4] S.C. Baker-Finch, K.R. McIntosh, D. Yan, K.C. Fong, T.C. Kho, Near-infrared free carrier absorption in heavily doped silicon, J. Appl. Phys. (2014) 116.

[5] D.A. Clugston, P.A. Basore, Modelling free-carrier absorption in solar cells, Prog. Photovolt. 5 (1997) 229–239.

[6] M.R. Vogt, H. Holst, M. Winter, R. Brendel, P.P. Altermatt, Numerical modeling of c-Si PV modules by coupling the semiconductor with the thermal conduction, convection and radiation equations, Energy Procedia 77 (2015) 215–224, http://dx.doi.org/10.1016/j.egypro.2015.07.030.

[7] I.G. Romijn, B.B.Van Aken, J. Anker, A.R.Burgers, A.Gutjahr, B.Heurtault, M. Koppes, E.Kossen, M.Lamers, D.S.Saynova, C.J.J.Tool, L.Fang, X.Jingfeng, L.Gaofei, X.Zhuo, W.Hongfang, H.Zhiyan, P.R.Venema, A.H.G.Vlooswijk, Industrial implementation of efficiency improvements in n-type solar cells and modules, in: Proceedings of the 27th European Photovoltaic Solar Energy Conference and Exhibition, 2012, pp. 533–537.

[8] M.K. Stodolny, G.J.M. Janssen, B.B. Van Aken, C.J.J. Tool, M.W.P.E. Lamers, I.G. Romijn, P.R. Venema, M.R. Renes, O. Siarheyeva, E.H.A. Granneman, J. Wang, J. Ma, J. Cui, F. Lang, Z. Hu, J. Löffler, PID- and UVID-resistant n-type solar cells and modules, in: Proceedings of the 32nd European Photovoltaic Solar Energy Conference Exhibition, 2016, pp. 1908–1911.

[9] Y. Komatsu, V.D. Mihailetchi, L.J. Geerligs, B. van Dijk, J.B. Rem, M. Harris, Homogeneous p+ emitter diffused using boron tribromide for record 16.4% screen-printed large area n-type mc-Si solar cell, Sol. Energy Mater. Sol. Cells 93 (2009) 750–752, http://dx.doi.org/10.1016/J.SOLMAT.2008.09.019.

[10] International Electrotechnical Commission, IEC 60904-1, Photovoltaic Devices, Part 1: Measurement of Photovoltaic Current–Voltage Characteristics, 2006.

[11] B.B. Van Aken, M.J. Jansen, A.J. Carr, G.J.M. Janssen, A.A. Mewe, Relation between indoor flash testing and outdoor performance of bifacial modules, in: Proceedings of the 29th European Photovoltaic Solar Energy Conference, 2014, pp. 2399–2402.

[12] V.D. Mihailetchi, J. Jourdan, A. Edler, R. Kopecek, R. Harney, D. Stichtenoth, J. Lossen, T.S. Böscke, H. Krokoszinski, Screen printed n-type silicon solar cells for industrial application, in: Proceedings of the 25th European Photovoltaic Sol. Energy Conference and Exhibition, 2010, pp. 1446–1448.

[13] A.R. Burgers, R.C.G. Naber, A.J. Carr, P.C. Barton, L.J. Geerligs, J. Xiong, G. Li, W. Song, H. An, Z. Hu, P.R. Venema, A.H.G. Vlooswijk, 19% efficient n-type Si solar cells made in pilot production, in: Proceedings of the 25th European Photovoltaic Solar Energy Conference and Exhibition, 2010, pp. 1106–1109.

[14] E.S. Roest, W. Nawara, B.B.Van Aken, Single side versus double side illumination method IV measurements for several types of bifacial PV modules, in: Proceedings of 33rd European Photovoltaic Solar Energy Conference and Exhibition, 2017, pp. 1427–1431 〈http://dx.doi.org/10.4229/EUPVSEC.20172017-5CO.7.1〉.

[15] P. Hoang, V. Bourdin, Q. Liu, G. Caruso, V. Archambault, Coupling optical and thermal models to accurately predict PV panel electricity production, Sol. Energy Mater. Sol. Cells 125 (2014) 325–338, http://dx.doi.org/10.1016/J.SOLMAT.2013.11.032.